Article

The crossregulation between ERK and PI3K signaling pathways determines the tumoricidal efficacy of MEK inhibitor

Jae-Kyung Won[1,2,†], Hee Won Yang[3,†], Sung-Young Shin[4,†], Jong Hoon Lee[4], Won Do Heo[3,*], and Kwang-Hyun Cho[1,4,*]

[1] Graduate School of Medical Science and Engineering, Korea Advanced Institute of Science and Technology (KAIST), Daejeon 305-701, Korea
[2] Molecular Pathology Center, Seoul National University Cancer Hospital, Seoul 110-744, Korea
[3] Department of Biological Sciences, Korea Advanced Institute of Science and Technology (KAIST), Daejeon 305-701, Korea
[4] Department of Bio and Brain Engineering, Korea Advanced Institute of Science and Technology (KAIST), Daejeon 305-701, Korea
[†] These authors contributed equally to this study.
[*] Correspondence to: Kwang-Hyun Cho, E-mail: ckh@kaist.ac.kr; Won Do Heo, E-mail: wdheo@kaist.ac.kr

MEK inhibitor has been highlighted as a promising anti-tumor drug but its effect has been reported as varying over a wide range depending on patho-physiological conditions. In this study, we employed a systems approach by combining biochemical experimentation with *in silico* simulations to investigate the resistance mechanism and functional consequences of MEK inhibitor. To this end, we have developed an extended integrative model of ERK and PI3K signaling pathways by considering the crosstalk between Ras and PI3K, and analyzed the resistance mechanism to the MEK inhibitor under various mutational conditions. We found that the phospho-Akt level under the Raf mutation was remarkably augmented by MEK inhibitor, while the phospho-ERK level was almost completely repressed. These results suggest that bypassing of the ERK signal to the PI3K signal causes the resistance to the MEK inhibitor in a complex oncogenic signaling network. We further investigated the underlying mechanism of the drug resistance and revealed that the MEK inhibitor disrupts the negative feedback loops from ERK to SOS and GAB1, but activates the positive feedback loop composed of GAB1, Ras, and PI3K, which induces the bypass of the ERK signal to the PI3K signal. Based on these core feedback circuits, we suggested promising candidates for combination therapy and examined the improved inhibitory effects.

Keywords: systems biology, mathematical model, ERK pathway, PI3K pathway, MEK inhibitor, resistance, robustness, biochemical control analysis

Introduction

Several targeted inhibitors blocking a specific signaling molecule have recently been spotlighted as having proved to be effective in the treatment of some kinds of tumors, opening the era of personalized cancer therapy (Rinehart et al., 2004; Adjei et al., 2008; LoRusso et al., 2010). However, those drugs as well as newly developed inhibitors have been found to become ineffective due to emerging resistance (Janne et al., 2009; Knight et al., 2010).

Resistance to cancer therapeutics can be divided into two categories: 'de novo' and 'acquired' (Meads et al., 2009). Acquired resistance in oncology refers to the acquisition of resistant phenotype, which means the progression of a tumor that had previously responded to treatment, largely owing to successive genetic changes. *De novo* resistance denotes immediate resistance to initial treatment through pre-existing mutations (intrinsic) or interactions between tumor cells and microenvironments (extrinsic) (Janne et al., 2009). Recent advancement of our understanding on complex biological networks from a systems view indicates that network's property contributing to the robustness is an important part of *de novo* resistance (Kitano, 2007).

The Ras-Raf-MEK-ERK signaling pathway (shortly ERK pathway) has been well known as a crucial oncogenic pathway, and inhibitors targeting this pathway have been vigorously developed (Brown et al., 2007; Yeh et al., 2007). But MEK inhibitor, which blocks the kinase activity of MEK, showed very low efficacy in several clinical trials (Rinehart et al., 2004; Haura et al., 2010). Recently, it has been reported that several types of cancers which have BRAF mutation are sensitive to MEK inhibitor (Solit et al., 2006; Wickenden et al., 2008) but its effect is very limited due to its drug resistance. Regarding the ERK pathway, several mechanisms of acquired resistance, such as the amplification of KRAS and BRAF, and mutations of MEK1 and NRAS have been discovered (Montagut et al., 2008; Emery et al., 2009; Corcoran et al., 2010; Nazarian et al., 2010); however, the mechanism of *de novo* resistance has not been well understood. Only

the relevance of the PI3K pathway in *de novo* resistance has been reported (Gopal et al., 2010; Iadevaia et al., 2010).

The ERK and PI3K pathways functionally co-regulate the same transcription factors which are associated with cell cycle and survival (e.g. cyclin D), and structurally regulated by various crosstalks and feedbacks (Mendoza et al., 2011). Highly interlinked biological network systems such as the ERK and PI3K pathways are reported to have the robustness to external perturbations (Lehar et al., 2008). In a large complex metabolic network, for example, the reorganization of metabolic fluxes utilizing alternative routes is an important mechanism for compensating the dysfunction of enzymes (Wagner, 2000). To get a fundamental understanding on the mechanism of drug resistance in a highly complex cellular signaling network, a new paradigm of systems approach is required.

In this study, we employed a systems approach that combines mathematical modeling and wet biological experimentation to investigate the underlying mechanism of drug resistance in the ERK and PI3K signaling network. From *in silico* analysis and biochemical experiments under various mutation conditions, we found that the phospho-Akt levels were remarkably increased by the MEK inhibitor in the BRAF mutation case. Moreover, our experiments showed that combined blockage of the ERK and PI3K pathways significantly decreased cell viability compared with single target inhibition. The biochemical control analysis (metabolic control analysis) and signal flux analysis clarified that Akt activation by EGF, normally fulfilled with GAB1 (Grb2-associated binding protein 1), is reinforced with the activation of the crosstalk between Ras and PI3K in response to MEK inhibitor treatment. MEK inhibitor disrupts the negative feedback loops from ERK to SOS (Son of Sevenless) and GAB1, but activates the positive feedback loop of GAB1 → Ras → PI3K → GAB1, which allows to bypass the ERK signal through the PI3K signaling pathway. This result suggests that the reorganization of the signaling flux causes the drug resistance to the MEK inhibitor. On the basis of such core feedback circuits for signal flux redistribution, we further identified promising drug candidates for combination therapy that can overcome the resistance to the MEK inhibitor and verified the resulting improved inhibitory effect through RNAi experiments.

Results

Developing a mathematical model of the ERK and PI3K signaling network

To investigate the underlying mechanism of MEK inhibitor resistance, we have employed the mathematical model developed by Kholodenko (Borisov et al., 2009) and further extended it by including the crosstalk of Ras-GTP with PI3K and the more detailed mechanism of EGFR in association with its downstream molecules since the direct interaction of PI3K with Ras-GTP has been observed in many experiments and the interaction of EGFR with its downstream partners has been reported to be essential in causing drug resistance (Mirzoeva et al., 2009; Prahallad et al., 2012). For instance, the kinase activity of PI3K has been known to be enhanced through direct binding of its catalytic subunit with Ras-GTP (Rodriguez-Viciana et al., 1994; Pacold et al., 2000; Suire et al., 2002). In addition, the phosphorylated receptor tyrosine kinase recruits and activates its downstream signaling molecules that

contain SH2 (Src homology domain 2) or PTB (phosphotyrosine-binding domain) independent of association with other binding partners as it has multiple autophosphorylation sites (Sordella et al., 2004; Lemmon and Schlessinger, 2010). All these are included in our extended model (Figure 1A, see also the mathematical model in Supplementary material for details).

Our extended mathematical model was further validated through experimentation using HEK293 cells that were also used in the Kholodenko model (Borisov et al., 2009). In particular, the pleckstrin homology (PH) domain of Akt (PIP$_3$ biosensor, PH$_{Akt}$) and ERK were used to monitor the PI3K and ERK activities based on the relative increase in the plasma membrane and nucleus. Cells were co-transfected with cyan fluorescent protein (CFP)-PH$_{Akt}$ and ERK-yellow fluorescent protein (YFP). After EGF stimulation, CFP-PH$_{Akt}$ was translocated to the plasma membrane within a minute and completely dissociated from the plasma membrane in 10 min, while ERK-YFP was translocated to the nucleus within 5 min and completely exported to the cytosol in 15 min (Figure 1B and C). When Ras was inhibited by the expression of dominant negative Ras (S17N), the translocation of ERK-YFP was completely blocked and the translocation of CFP-PH$_{Akt}$ to the plasma membrane was also significantly reduced. We further confirmed that constitutively active Ras (G12V) induced significant translocation of PH$_{Akt}$ to the plasma membrane (Supplementary Figure S1), which supports the presence of the crosstalk from Ras to PI3K.

Our mathematical model consists of 58 ordinary differential equations and 136 kinetic parameters. Most kinetic parameter values were taken from the original model (Borisov et al., 2009) and other parameter values of newly added or modified reactions were estimated based on the previous experimental data (Borisov et al., 2009). In general, the simulation results of a mathematical model might highly depend on the parameter choice due to limited experimental data resulting in an ill-posed parameter optimization problem. Thus, to evaluate the robustness of our results, we further carried out extensive simulations repetitively ($n = 30$) over up to 50% random variation of parameter values selected from a log-uniform distribution and confirmed that the responses of the ERK-PI3K signaling network (i.e. Ras-GTP, phospho-ERK, phospho-Akt, and phospho-GAB1) are robust to such parameter variations (Supplementary Figure S2).

The effect of the MEK inhibitor in diverse mutation conditions

To simulate the effect of MEK inhibitor in diverse mutation conditions, we considered three single and three combined mutation cases (six different mutation cases in total). In these simulations, we assumed that the MEK inhibitor decreases the MEK phosphorylation level up to 80% to reflect the real inhibitory intensity (Iverson et al., 2009). To quantify the effect of the MEK inhibitor, we investigated the area under curve (AUC) of the time trajectories of phospho-Akt and phospho-ERK after EGF stimulation and compared the percent change of AUC before and after the application of the MEK inhibitor.

The simulation results showed that, in the single mutation cases (i.e. Ras, Raf, and PI3K), the phospho-ERK levels were substantially decreased by the MEK inhibitor, while the phospho-Akt levels were quite different depending on mutation cases: the increments of the phospho-Akt level were relatively small in the
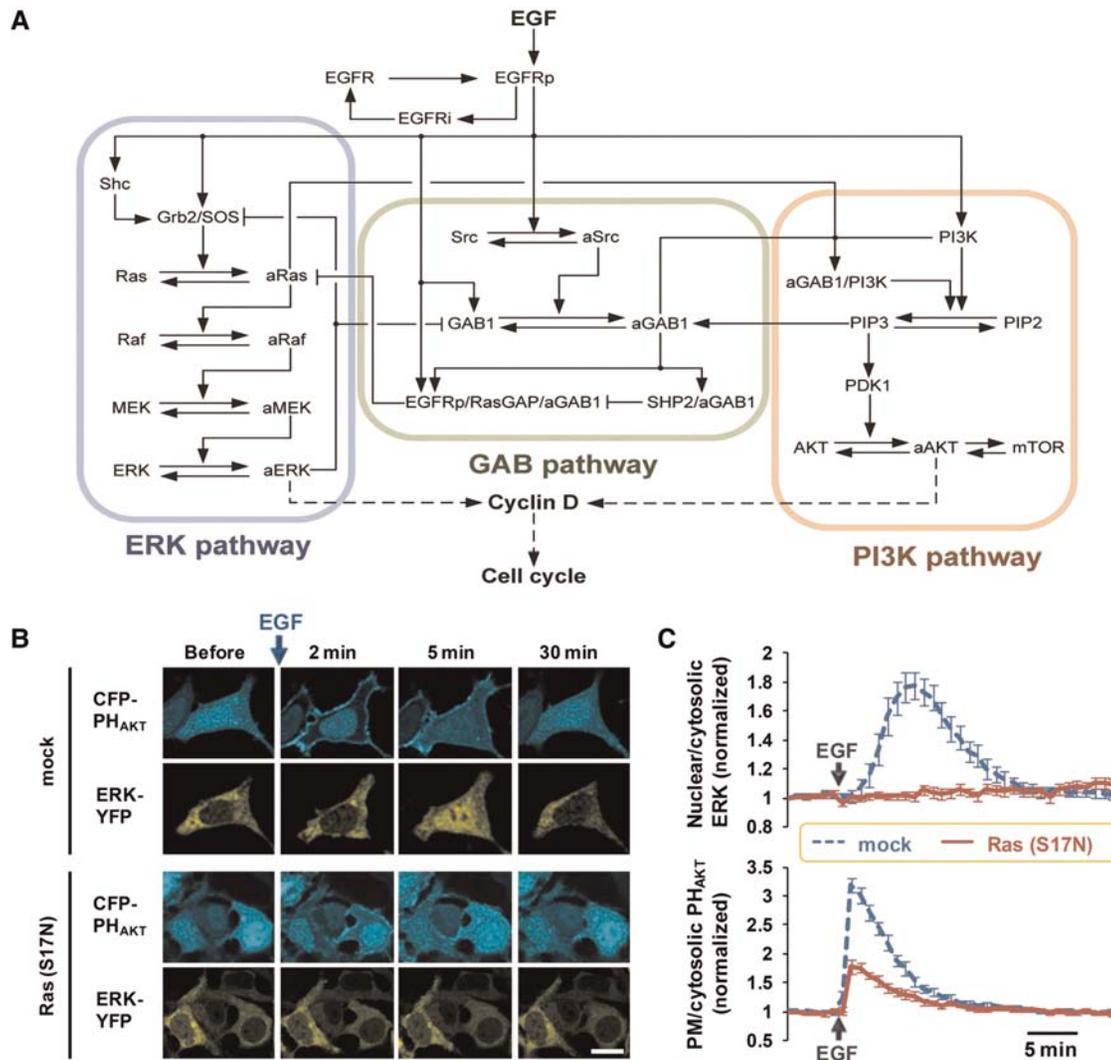
Figure 1 The reconstruction of the ERK and PI3K signaling network and experimental validation. (**A**) The scheme of combined signaling network of Ras-Raf-MEK-ERK and PI3K-Akt pathways. The reactions are described in Section IV of Supplementary material. (**B**) After EGF (10 nM) stimulation, CFP-PH$_{Akt}$ and ERK-YFP are translocated to the plasma membrane and nucleus, respectively. This translocation of CFP-PH$_{Akt}$ and ERK-YFP is remarkably decreased or completely blocked, respectively, in the cells expressing Ras (S17N). Scale bar represents 20 μm. (**C**) Quantitative measurement of the ratio of nuclear to cytosolic ERK and plasma membrane to cytosolic PH$_{Akt}$ (normalized to the initial value) in **B**. Data represent the mean $\pm$ SEM ($n > 10$).

Ras and PI3K mutation cases, whereas the increments were remarkable in the Raf mutation case (Figure 2A). In combined mutation cases, the increments of the phospho-Akt level by the MEK inhibitor were relatively small compared with the single mutation cases; however, in the Ras and Raf mutation condition, the phospho-level change of Akt was relatively outstanding (Figure 2A). To validate these simulation results under various mutational conditions, we further carried out additional experiments using HEK293 cells. To mimic mutational condition of Ras, BRAF, and PI3K, we used Ras (G12V), BRAF (V600E), and p110-CAAX, either alone or in combination. All these experimental results were well in accord with the simulation results (Figure 2B and C, Supplementary Figures S3−S5). In summary, the change of the phospho-Akt levels by the MEK inhibitor was most prominent under the Raf mutational condition. On the other hand, such level change under other mutational conditions was relatively small

since Akt was intrinsically activated prior to the treatment of the MEK inhibitor. Taken together, these results suggest that, even in the BRAF mutational condition, the effect of the MEK inhibitor on the ERK signal can be compensated by augmented PI3K signal.

PI3K-Akt activation can lead to the resistance to MEK inhibitor in BRAF-mutant melanoma cells

To investigate whether PI3K-Akt activation is related to the resistance to MEK inhibition in BRAF-mutant cancer cells, we conducted experiments with BRAF-mutant melanoma cell line. First, to examine the effect of MEK inhibition on the PI3K activity in BRAF-mutant cancer cell line, we measured the phospho-Akt level in SK-Mel-1 or SK-Mel-5 which are BRAF (V600E)-mutant suspension or adhesion cells, respectively. Consistent with previous results shown in Figure 2, incubation with PD0325901 induced a significantly enhanced phospho-Akt level in both cell
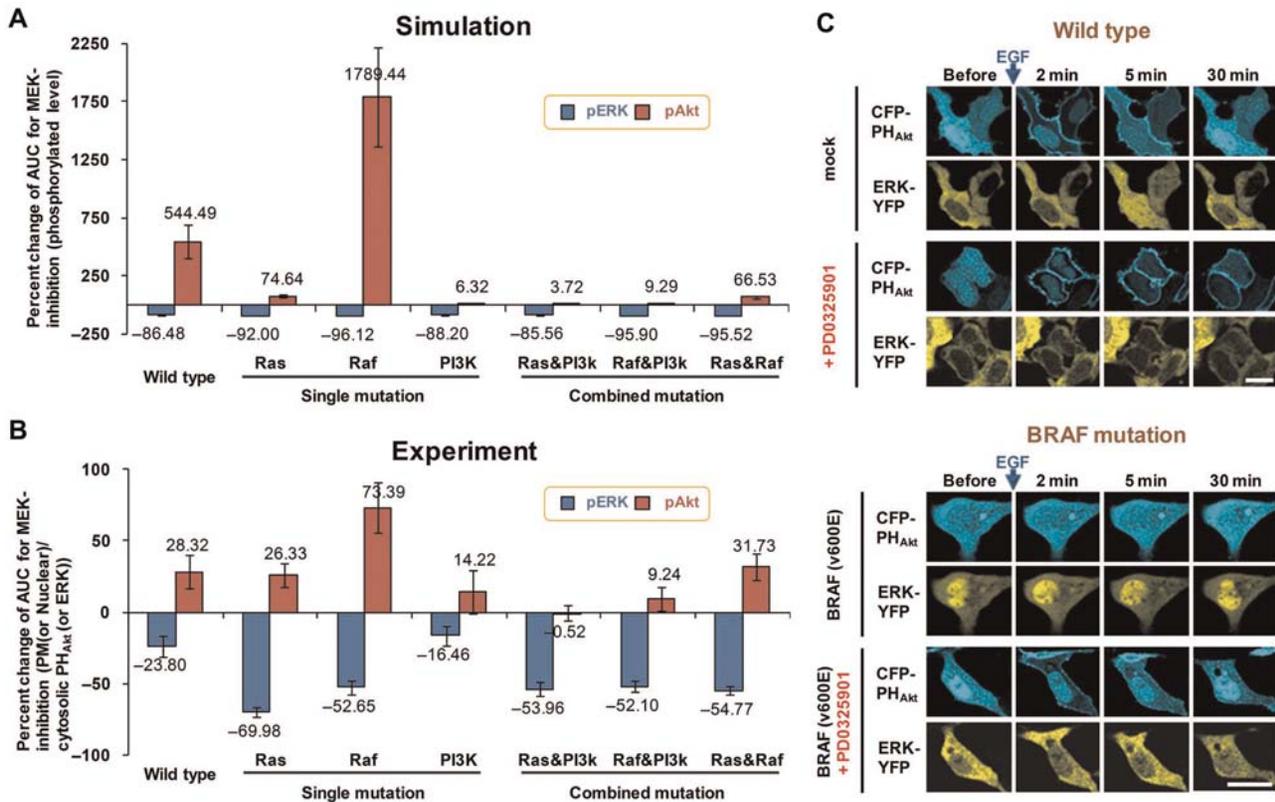
Figure 2 MEK inhibition causes the sustained PI3K activation. (**A**) A percent change in AUC for MEK inhibitor, which is defined as the difference between the AUCs of the phospho-Akt (or phospho-ERK) before and after MEK inhibitor treatment normalized with respect to the AUC of the phospho-Akt (or phospho-ERK, respectively) before MEK inhibitor treatment. AUC was calculated using the time course data of the phospho-ERK and -Akt shown in Supplementary Figures S4B (single mutation cases) and S5B (combined mutation cases). Data represent the means of repetitive simulation trials ($n = 30$) with 30% random perturbation of parameter values. Each error bar indicates the standard error. The blue bar (the negative values) indicates the phospho-ERK level and the red bar (the positive values) indicates the phospho-Akt level. (**B**) The percent change in AUC for MEK inhibitor treatment (Experiment). AUC was calculated using the time course data of the phospho-ERK and -Akt shown in Supplementary Figures S4B (single mutation cases) and S5B (combined mutation cases). Experimental measurements denote the ratio of nuclear to cytosolic ERK and the ratio of plasma membrane to cytosolic PH$_{Akt}$, after 30 min from EGF (10 nM) stimulation. Data represent the mean $\pm$ SEM ($n > 10$). (**C**) After EGF (10 nM) stimulation, the translocation of CFP-PH$_{Akt}$ is sustained in the cells pre-incubated with PD0325901 (50 nM) for 30 min. The expression of BRAF (V600E) inhibits EGF (10 nM) induced translocation of CFP-PH$_{Akt}$ and it is released by pre-incubation of PD0325901 (50 nM) for 30 min. Scale bar represents 20 μm.

lines (Figure 3A).

Observing the enhancement of the PI3K activity in BRAF-mutant cell lines, we hypothesized that inhibiting the PI3K activity might restore sensitivity to PD0325901. To test this hypothesis, we treated SK-Mel-1 and SK-Mel-5 with increasing concentrations of PD0325901 or the PI3K inhibitor, LY294002, alone or in combination. They were much more sensitive to the combination than treatment with either compound alone (Figure 3B), suggesting that PI3K-Akt activation causes the *de novo* resistance to MEK inhibitor, which can be overcome by combinatorial targeting of PI3K and MEK.

To test whether combined MEK and PI3K inhibition finally induces SK-Mel-1 and SK-Mel-5 death, we investigated the combinatorial effect of PD0325901 and LY294002 on enhancing the cell death. In accord with the viability test, while combinatorial inhibition induced significant cell death, neither PD0325901 nor LY293002 alone caused a substantial increase in cell death (Figure 3C and D). Moreover, although none of LY294002 or

PD0325901 had an effect on cell proliferation in SK-Mel-1 and SK-Mel-5, combinatorial inhibition showed a synergistic effect on cell proliferation (Figure 3E). Taken together, these results suggest that Akt activation by the MEK inhibitor treatment plays an important role in the *de novo* resistance to the MEK inhibitor in BRAF-mutant cancer cell lines.

MEK inhibitor reorganizes the signal flux of the ERK and PI3K pathways

To identify the key molecular mechanism conferring resistance to MEK inhibition, we applied biochemical control analysis (metabolic control analysis, MCA) and quantitatively evaluated the influence of any biochemical reaction or signaling component on the ERK and PI3K signaling. In this study, we employed two criteria, response coefficient analysis (RCA) and control coefficient analysis (CCA) (Wildermuth, 2000). RCA measures the change in the steady-state level to sufficiently small parameter perturbation and CCA measures the steady-state value to the perturbation of an individual reaction rate (denoted by 'a process'; see section
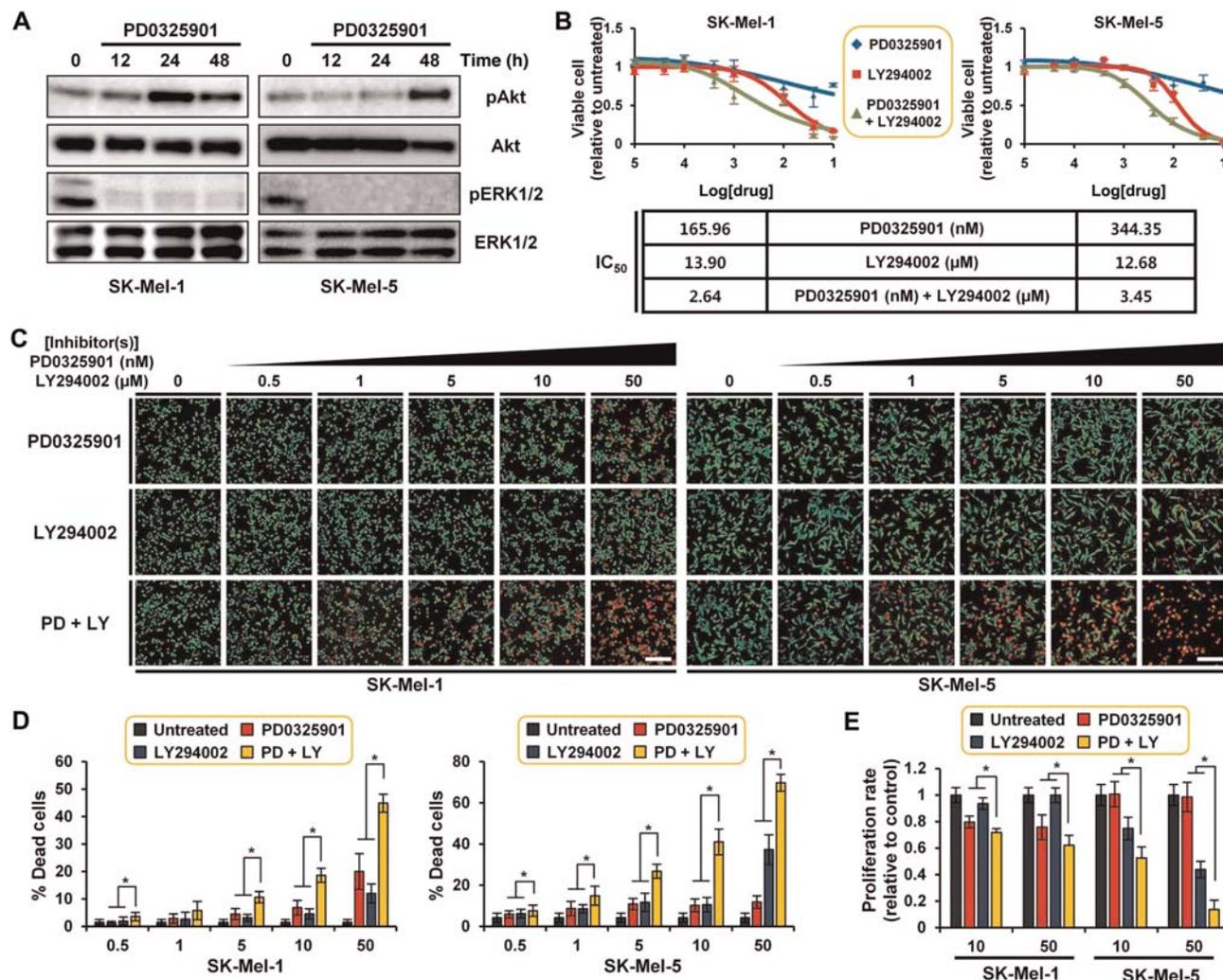
Figure 3 Combined blockage of PI3K-Akt activation shows the synergistic effects suggesting the role of PI3K pathway for the resistance to MEK inhibitor in BRAF-mutant melanoma cells. (**A**) Western blotting analysis of SK-Mel-1 and SK-Mel-5 following the treatment with PD0325901 (50 nM). Time point is indicated above the phospho-Akt. (**B**) SK-Mel-1 and SK-Mel-5 cells were treated with the indicated concentrations for 48 h and cell viability was determined. Cell viability is shown relative to the untreated control. The IC_{50} for PD0325901 or LY294002 alone and in combination are shown in a tabular form. (**C**) Live/dead assays of SK-Mel-1 or SK-Mel-5 cells treated with the indicated concentrations of PD0325901 or LY294002 alone or in combination for 48 h. The cells were double stained with Calcein AM and ethidium homodimer-1 (EthD-1). The Calcein AM and EthD-1 mixture show live cells in green and dead cells in red, respectively. Scale bar represents 20 μm. (**D**) Quantitative measurements of dead cell percentage. Data represent the mean ± SD ($n > 10$, at least >2000 cells were counted). *$P < 0.001$. (**E**) Cell number was counted after 48 h from the treatment of each inhibitor alone and in combination. The proliferation rate is shown relative to the untreated control. Data represent the mean ± SD ($n > 10$). *$P < 0.001$.

Materials and methods for details). In this analysis we considered various biological contexts including three single and three combined mutation cases as well as treatment of MEK inhibitor.

In RCA, we found that four signaling molecules, PDK1, Akt, PI3K, and GAB1 had the most dominant effect on Akt activation in the wild-type (WT), Ras, and Raf mutation cases (the left panel of Figure 4A and Supplementary Figure S6A). In the PI3K mutation case, PDK1, Akt, and mTOR had the dominant effect. Interestingly, we found that the effect of Grb2/SOS (shortly GS complex), SHP2, and RasGAP changed their sign in the MEK inhibitor cases (the left panel of Figure 4A, indicated by asterisk). For example, the GS complex and SHP2 played a negative role for the Akt activation in the absence of the MEK inhibitor but its

role was switched to a positive one when the MEK inhibitor is present. The functional role of RasGAP was switched to a negative one after MEK inhibition. On the ERK activation, the GS complex and RasGAP had relatively dominant roles, but their functional effects were not changed for the MEK inhibition in contrast to the cases of Akt activation (Figure 4A, right panel, and Supplementary Figure S6B).

To identify the influential biochemical processes on the Akt and ERK activation, we carried out CCA repetitively ($n = 30$) over 10%, 20% and 30% random variation of parameter values (selected from a log-uniform distribution), respectively. For illustration, we scored each process by its frequency ranked in top 10% of each CCA. For instance, if the process va44 was ranked in top
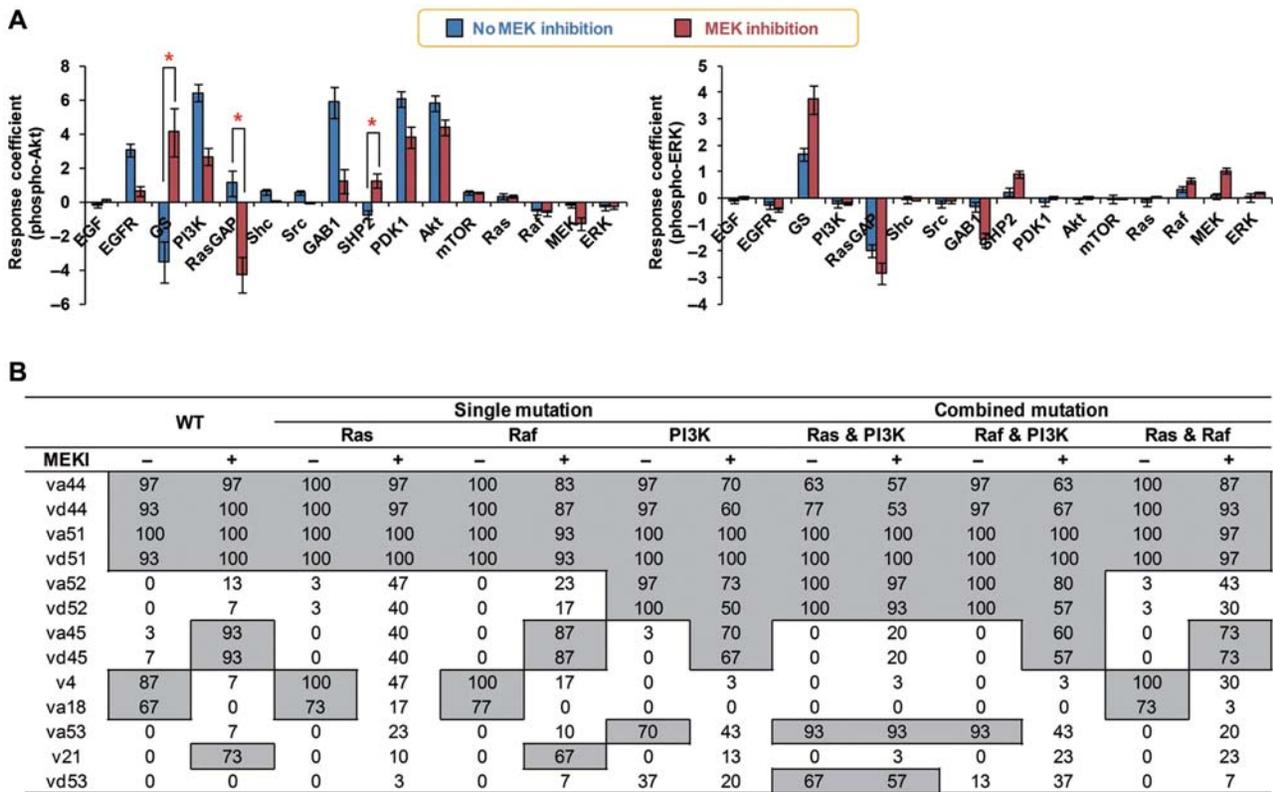
Figure 4 Biochemical control analysis. (**A**) RCA (WT case). Data represent the means of repetitive simulation trials ($n = 30$) with 30% random perturbation of parameter values. Each error bar indicates the standard error. The blue bar indicates the response coefficient in the absence of the MEK inhibitor and the red bar in the presence of the MEK inhibitor. Asterisk indicates the change in the functional effect before and after MEK inhibitor treatment. (**B**) CCA. Data represent the frequency (i.e. how many times the selected process is ranked in top 10% of each CCA). For instance, va44 was ranked in top 10% for 29 times over 30 CCAs, so it has the value of 97. Data were obtained by repetitive CCAs ($n = 30$) over 20% random perturbation of parameter values.

10% for 29 times over 30 CCAs, then va44 has the value of 97. Through this analysis, we found that the processes va44 (production of PIP3), vd44 (dephosphorylation of PIP3), va51 (phosphorylation of Akt by PDK1) and vd51 (dephosphorylation of phospho-Akt) were most influential on the Akt activation, irrespective of mutation conditions and MEK inhibitor treatment (Figure 4B and Supplementary Tables S1–S3). The processes v4 (receptor internalization) and va18 (phosphorylation of mGAB1 by the receptor complex (Rp) and Src) had influential roles in the Akt activation under the WT, Ras, and Raf mutations in the absence of the MEK inhibitor but their effects disappeared by MEK inhibitor while the effects of va45 and vd45 became remarkable by MEK inhibitor under WT, Ras, and PI3K mutations. From the additional simulations, we also found that MEK inhibitor have changed the functional effect of biochemical processes such as v22, va54, vd54, v19, v23, v30, va45, and vd45 on the Akt activation in the WT case and the functional effect of v22, va54, vd54, v3, v4, and va18 in the Raf mutation case (Supplementary Table S7), which means that the effect of each process on Akt activation can be switched from negative to positive or vice versa by MEK inhibitor. For example, the association of GAB1 with SHP2 (v22) has the role of decreasing Akt activation as suggested by Mattoon et al. (2004); however, its role changes from negative to positive in the MEK inhibitor case, which

shows that the RCA and CCA results are well in accord with each other. Taken together, we infer that the reactions showing positive effects consistently, such as PDK1, Akt, PI3K, and GAB1, constitute a common pathway of signal flux for pAkt irrespective of MEK inhibitor treatment, while Grb2/SOS, SHP, and Ras-GAP showing a 'switching role' are involved in turning on the alternative routes for pAkt after MEK inhibition (Figure 4A).

To verify our inference and further investigate the signal flux change by MEK inhibitor, we have investigated the activities of Akt upstream signal molecules. PI3K is a direct upstream signal of Akt and it is also stimulated by two upstream signals: one is through Ras-GTP and the other is through phosphor-tyrosine residues from EGFR and GAB1. The analysis result shows that the major signal increase of PI3K in the case of MEK inhibition was due to Ras-GTP (Supplementary Figure S7, left panel). We have further analyzed the increase of Ras-GTP stimulated by Grb2-SOS which has two upstream signals: one is directly through EGFR and the other is through GAB1. In this case, the major signal change of Ras was through GAB1 (Supplementary Figure S7, right panel). From these results, we found that Ras-GTP and GAB1 play a major role in the signal flux change by the MEK inhibitor and constitute the activation loop of GAB1$\rightarrow$SOS$\rightarrow$RasGTP$\rightarrow$PI3K$\rightarrow$GAB1 (Figure 5). To further examine these results and visualize such signal flux changes caused by MEK inhibition, we calculated the
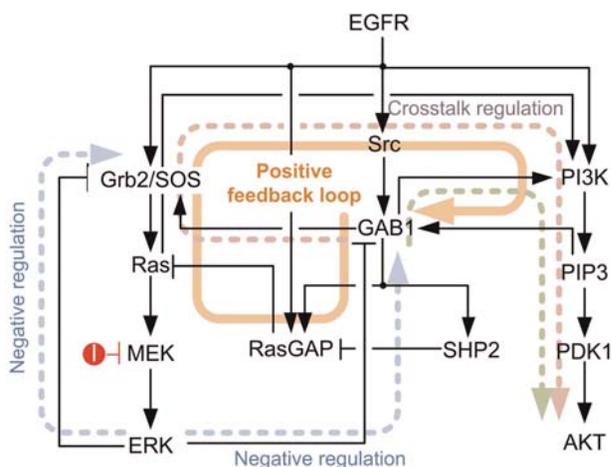
Figure 5 The reorganization of signal flux evoked by the MEK inhibitor treatment. Sandy brown-colored line indicates the newly activated route of EGF signal in response to MEK inhibition, which leads to the sustained activation of Akt. Light blue-colored line denotes the negative feedback loops which are disrupted by MEK inhibitor and light green-colored line shows the nominal route of Akt activation.

percent changes in signal flux and signal strength before and after MEK treatment under the three single and combined mutation cases as well as WT case (see section Materials and methods and Supplementary Figures S8–S14 for details). As a result, we could identify a significant increase in signal flux along the feedback loop of mGAB1→SOS→RasGTP→PI3K→mGAB1 particularly for WT and Raf mutation cases (Supplementary Figures S8 and S10). The emergence of such an alternative route for signal flux originates from the weakening of negative feedback from ERK to SOS and GAB1 by MEK inhibitor, which subsequently reinforces the crosstalk effect from Ras-GTP to PI3K. The switching role of RasGAP and SHP2 is mostly due to their complex formation with GAB1 since those complexes play a partial role in the activation of Ras.

In summary, MEK inhibitor treatment diversifies the signal flux for Akt activation with the activation of the positive feedback loop including the crosstalk between Ras-GTP and PI3K (Figure 5). This demonstrates a mechanism with which a biological network maintains its robustness to perturbations: signal flux reorganization through the activation of alternative pathways.

In silico experiments for combinatorial strategies

The concept of combination therapy is receiving significant attention for personalized medicine. In this section, we analyze the combinatorial effect of the MEK inhibitor and other potential drug targets. Here, we have chosen three candidate molecules: PDK1, SOS, and GAB1, which play a central role in the signal flux change (Figure 4). To quantitatively measure the combinatorial effect we simulated the phospho-Akt levels by gradually increasing the MEK inhibitor and each potential drug target at the same time. The simulation results show that the pAkt level became monotonically decreased along with the decrement of PDK1 irrespective of the intensity of the MEK inhibitor (Figure 6A). In the case of SOS, the pAkt level was sharply decreased in a very narrow range of SOS and this response pattern was constant over all the range of the MEK inhibitor (Figure 6B). The response curve to GAB1 was quite different depending on the intensity of MEK inhibitor.

The level of pAkt was monotonically decreased along with the GAB1 concentration for a weak intensity of the MEK inhibitor but it showed a multi-phasic response for a strong MEK inhibitor: beyond a certain threshold level of GAB1, pAkt monotonically decreased but, in a very narrow range of GAB1, it sharply increased and decreased (Figure 6C). To understand this unexpected response pattern with respect to GAB1, we analyzed the signaling network and identified that GAB1 regulates Akt activation through an incoherent feedforward loop (a positive regulation link composed of the SOS/Grb2 complex and a negative regulation link composed of RasGAP) and a negative feedback loop (composed of the ERK pathway; Figure 6D). When MEK inhibitor blocks the negative feedback loop, the positive regulation link is activated and thus pAkt levels become increased. However, when the GAB1 level increases beyond a certain threshold value, the negative regulation link turns on and the increment of pAkt is suppressed (see Supplementary Figure S16 for details).

From these simulation results, we have new insights into the strategies of combination therapy. First, the response curve to drug candidates can dramatically be changed depending on the intensity of the MEK inhibitor. Secondly, *in silico* analysis allows us to predict the different efficacy of combination therapies.

In our simulation results, GAB1 is not only the key mediator of the positive feedback loop that causes the increase in signal flux to PI3K under MEK inhibition as we found in the previous section, but also a promising drug target for combination therapy with the MEK inhibitor. To further verify this, we designed additional experiments and conducted them. We blocked the expression of GAB1 using RNAi (Supplementary Figure S15) in the cell expressing BRAF (V600E) and pre-incubated with PD0325901. Then, we monitored the translocation of YFP-PH$_{Akt}$ induced by EGF stimulation. After EGF stimulation, the inhibition of MEK by PD0325901 rescued the translocation of YFP-PH$_{Akt}$ which was blocked by ERK activation under the BRAF mutational condition whereas the inhibition of GAB1 expression showed a significant reduction in the translocation of YFP-PH$_{Akt}$ induced by EGF. These experimental results further support our conclusion (Figure 6E).

Discussion

There have been several studies about the resistance mechanism of the MEK inhibitor, but most of them focused on acquired resistance (Montagut et al., 2008; Emery et al., 2009; Corcoran et al., 2010; Nazarian et al., 2010). As acquired resistance arises from the genetic instability of cancer, it is difficult to predict its occurrence and pattern. On the other hand, to get drug-resistant phenotype, cancer cells may need *de novo* resistance to guarantee their viabilities before the emergence of acquired resistance. So, it is important to minimize such *de novo* resistance to lower the chance of acquired resistance, which is also related to the general robustness of a biological network.

Recently, some efforts have been made to understand the molecular mechanism conferring the *de novo* resistance to the MEK inhibitor in various cancer cell lines and the relevance of PI3K pathway was suggested (Mirzoeva et al., 2009; Gopal et al., 2010; Iadevaia et al., 2010). However, there has been no report
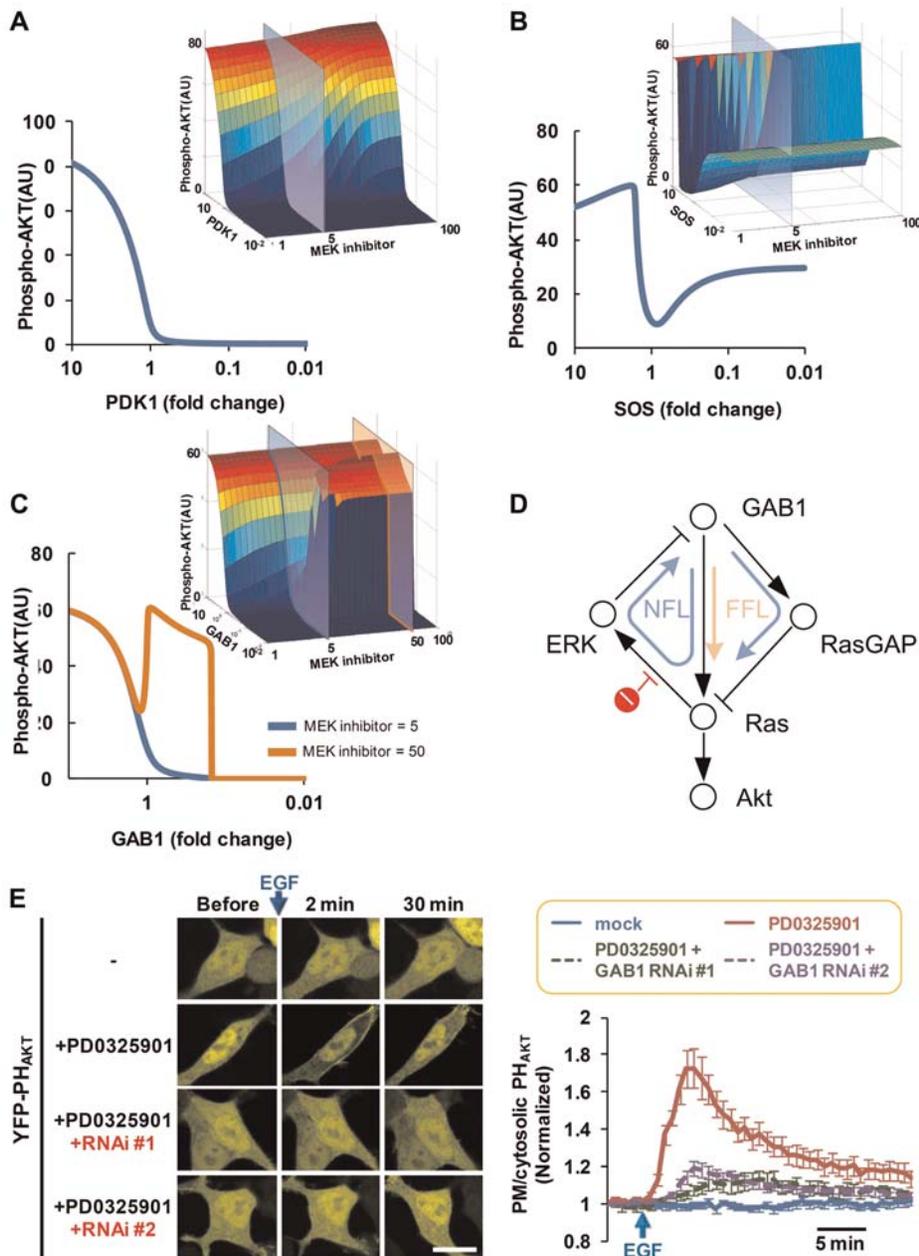
Figure 6 Steady-state response curves of pAkt amplitude for different concentration levels of other major molecules under MEK inhibition. (**A**–**C**) The steady-state level change of pAkt amplitude along with the concentration of PDK1 (**A**), SOS (**B**), GAB1 (**C**) respectively, under MEK inhibition. Blue line indicates the response curve of pAkt when inhibiting 80% of MEK and orange line for 98% inhibition of MEK. (**D**) The structure of signaling network responsible for the dynamic response of pAkt when lowering GAB1. (**E**) After EGF (10 nM) stimulation, the blockage of GAB1 expression by RNAi reduced the translocation of YFP-PH$_{Akt}$ in the cells expressing BRAF (V600E) and pre-incubated with PD0325901 (50 nM) for 30 min. Scale bar represents 20 μm (left panel). Quantitative measurement of the ratio of plasma membrane to cytosolic PH$_{Akt}$ (normalized to the initial value) in the right panel. Data represent the mean ± SEM ($n > 20$).

to date on the detailed mechanism of signaling dynamics based on system-level analysis of diverse mutational cases. In this study, we revealed that the effect of the MEK inhibitor can be quite different depending on mutational conditions. In addition, we unraveled the underlying mechanism and identified the core signaling circuit through which signal fluxes are redistributed. Furthermore, we presented promising potential drug targets for combination therapy that can overcome the resistance in issue

and verified the improved inhibitory effect through both *in silico* and wet experiments.

We showed that *de novo* resistance by Akt activation exists even in BRAF mutation melanoma cell lines known to be sensitive to the MEK inhibitor, which can be overcome by combination therapy with the PI3K inhibitor. In the case of BRAF mutation, the complex interactions among growth factors, intervention by drug, and the structure of signaling network can collectively

cause the reorganization of signal flux and result in 'extrinsic' *de novo* resistance, but, in the case of Ras, PI3K or combined mutations, Akt is usually being activated by such mutations and this leads to 'intrinsic' *de novo* resistance that was observed in previous studies (Engelman et al., 2008; Wee et al., 2009). Furthermore, using biochemical control analysis and signal flux analysis, we found that that MEK inhibitor enhances Akt activation through the crosstalk regulation between ERK and PI3K signaling pathways and redistributes the flux over the core signaling circuit composed of GAB1→Ras→PI3K→GAB1 in which the feedback suppressions of GAB1 and Ras are released by the MEK inhibitor. Moreover, we identified that the Grb2/SOS complex, SHP2, and RasGAP play a switching role in the redistribution of the signal flux (Figures 4 and 5).

Our simulation results provided a novel insight into the robustness of signal transduction systems and the drug resistance. For example, two negative feedback loops composed of ERK→SOS→Ras→ERK and ERK→GAB1→SOS→Ras→ERK compensate the upstream signals of the ERK pathway when MEK is suppressed by its specific inhibitor, which means that such feedback loops are one important mechanism of maintaining the robustness of signal flow. On the other hand, the crosstalk between ERK and PI3K pathways is also an important mechanism of preserving the robustness as it partly overlaps or compensates the disabled ERK pathway. Moreover, the positive feedback loop composed of GAB1→Ras→PI3K→GAB1 causes a digital-like response to EGF, which makes the system robust to the fluctuation of EGF (Kitano, 2007).

Targeted therapy usually aims at a specific protein of signaling pathway, which can be considered as perturbation to the underlying signaling network. It is known that a biological system is intrinsically robust against external perturbation and this property can be associated with resistance to target inhibition (Kitano, 2007; Lehar et al., 2008). Targeted therapy usually aims at a specific protein of signaling pathway, which can be considered as perturbation to the underlying signaling network. It is known that a biological system is intrinsically robust against external perturbation and this property can be associated with resistance to target inhibition (Kitano, 2007; Lehar et al., 2008). The mechanisms for biological robustness have been studied extensively in the field of metabolic network and such a concept can also be applied to signaling networks (Papp et al., 2011). In particular, signal flux reorganization emerging from various interactions between different molecules can be an important mechanism for *de novo* resistance.

In vivo cancer cells are usually exposed to a high concentration of growth factors including EGF which is released from themselves as well as extracellular matrices. If the MEK inhibitor is applied to cancer cells surrounded by a high level of growth factor, our study shows that the PI3K signaling might be immediately increased through signal flux redistribution and this can cause *de novo* resistance. Therefore, multi-target therapy is crucial to prevent such resistance and increase tumoricidal efficacy.

In summary, the proposed systems biology approach based on mathematical modeling and single cell experiment can be a useful framework for enhancing our understanding of molecular

mechanism conferring resistance to the MEK inhibitor and it provide a novel insight to rational combinatorial therapies. A larger-scale network model embracing all cancer-related genes and pathways remains as a further study for realization of personalized optimal therapy.

Materials and methods
Mammalian DNA constructs
CFP and YFP-PH$_{Akt}$ have been described previously (Shin et al., 2011). p110-CAAX was a gift from Lewis Cantley (Harvard Medical School). ERK-YFP was purchased from the Alliance for Cellular Signaling. mCherry-Ras (G12V and S17N) and mCherry-BRAF (V600E) were generated using PCR and subcloned into mCherry-C1 vector (Clonetech).

Reagents
EGF was from Calbiochem. PD0325901 (Cayman) and LY294002 (LC Laboratory) were dissolved in dimethyl sulfoxide (DMSO) and used at an indicated concentration. Rabbit anti-phospho-ERK1/2 (The202/Tyr024), anti-ERK1/2, and anti-phospho-Akt (Ser473) were from Cell Signaling. Rabbit anti-Akt was from Millipore. Secondary mouse anti-rabbit HRP-linked IgG antibodies were from GE Healthcare. A universal negative control and GAB1 specific RNAi (#1: 5′-AGUCUCUACACUCGAUGUC-3′; #2: 5′-UCUACCUAGA GUGGAAGUG-3′) were obtained from Invitrogen and Bioneer, respectively. Forty-eight hours after RNAi transfection (100 pM), cells were used for imaging.

Cell culture and electroporation
HEK293 (ATCC, No. CRL-1573) was cultured in Dulbecco's modified Eagle medium (DMEM) supplemented with 10% FBS and penicillin−streptomycin solution. SK-Mel-1 (KCLB, No. 30067) and SK-Mel-5 (KCLB, No. 30070) were cultured in RPMI1640 with 10% FBS and penicillin−streptomycin solution. Electroporation was performed using a Neon (Invitrogen) following the manufacturer's instructions. For HEK293 cell imaging, shocked cells were aliquotted into 96-well black plates with glass bottoms (Metrical). After 24 h, HEK293 cells were starved from 12 to 16 h in FBS-free medium and then used for imaging.

Imaging and microscopes
Before imaging, the medium was replaced with phosphate-buffered saline containing glucose (1 g/L; Invitrogen). All images were taken using a confocal microscope (A1R; Nikon). Images were analyzed using NIS (Nikon) and MetaMorph software (Molecular Devices).

Cell viability assay and IC$_{50}$
Cells were seeded at 10000 cells per well of a 96-well plate (Greiner Bio-One). After overnight incubation, the cells were treated in triplicate with serial dilutions of each drug for 48 h. Cell viability relative to untreated cells was determined with EZ-Cytox (Daeillab Service) according to the manufacturer's protocol and read on a microplate luminometer (BIO-RAD). The EZ-Cytox assay is based on water soluble tetrazolium salts. IC$_{50}$ (defined as the concentration required inhibiting cell viability to 50% of untreated control) was determined with a Matlab toolbox.

Live/dead cell assay
Cells were seeded at 20000 cells per well of a 96-well plate (Metrical). After overnight incubation, the cells were treated in

duplicate with serial dilutions of each drug for 48 h. And then, live and dead cells were determined with Live/Dead cell assay kit (Invitrogen) according to the manufacturer's protocol and captured using a confocal microscope (A1R, Nikon).

Statistical analysis

Statistical analyses were performed with Student's *t*-test (Figure 3B) and the analysis of variance (ANOVA) with Bonferroni's post test (Figure 3D and E). Significance was established for $P < 0.01$.

Mathematical modeling and computational analysis

Our mathematical model is extended based on the original one developed by Borisov et al. (2009) with some modifications and extension (see section Results for details). The modified and extended model is described in Supplementary Files (see Section IV of Supplementary material). We used the genetic algorithm and multiobjective function of Matlab for parameter estimation. The developed mathematical model was implemented, simulated, and analyzed with Matlab (R2010a, The MathWorks, Natick, MA).

The CCA result is represented by the control coefficient (of *i*th process) which is defined as follows:

$$C_i^{Y_j} = \frac{\partial \ln Y_j}{\partial \ln v_i} = \frac{v_i}{Y_j}\frac{\partial Y_j}{\partial v_i} \approx \frac{\Delta Y_j/Y_j}{\Delta v_i/v_i},$$

where i (or v_i) denotes the process number (see Section IV of Supplementary Information for details) and Y_j denotes the phospho-ERK or -Akt level at the steady state. The control coefficient is calculated for a small perturbation ($\Delta v_i/v_i = 10^{-3}$ in this case). The RCA result is represented by the response coefficient (of parameter P_i), which is defined as follows:

$$R_i^j = \frac{\partial \ln Y_j}{\partial \ln p_i} = \frac{p_i}{Y_j}\frac{\partial Y_j}{\partial p_i} \approx \frac{\Delta Y_j/Y_j}{\Delta p_i/p_i},$$

where we change the total amount of a signal molecule to perturb the parameter ($\Delta p_i/p_i = 10^{-3}$ in this case).

To calculate the percent change in the signal flux (ψ_i) before and after the MEK inhibitor treatment, we introduced the following measure:

$$\psi_i = \frac{\int_o^T v_i^p(t)\mathrm{d}t - \int_o^T v_i^a(t)\mathrm{d}t}{\int_o^T v_i^a(t)\mathrm{d}t} \times 100,$$

where '*p*' denotes the presence of the MEK inhibitor and '*a*' denotes the absence of it. The percent change in the signal strength (φ_j) before and after the MEK inhibitor treatment, was calculated as follows:

$$\varphi_j = \frac{\int_o^T X_j^a(t)\mathrm{d}t - \int_o^T X_j^a(t)\mathrm{d}t}{\int_o^T X_j^a(t)\mathrm{d}t} \times 100,$$

where X_j denotes the time profile of phospho-ERK or -Akt level.

Supplementary material

Supplementary material is available at *Journal of Molecular Cell Biology* online.

References

Adjei, A.A., Cohen, R.B., Franklin, W., et al. (2008). Phase I pharmacokinetic and pharmacodynamic study of the oral, small-molecule mitogen-activated protein kinase kinase 1/2 inhibitor AZD6244 (ARRY-142886) in patients with advanced cancers. J. Clin. Oncol. *26*, 2139–2146.

Borisov, N., Aksamitiene, E., Kiyatkin, A., et al. (2009). Systems-level interactions between insulin-EGF networks amplify mitogenic signaling. Mol. Syst. Biol. *5*, 256.

Brown, A.P., Carlson, T.C., Loi, C.M., et al. (2007). Pharmacodynamic and toxicokinetic evaluation of the novel MEK inhibitor, PD0325901, in the rat following oral and intravenous administration. Cancer Chemother. Pharmacol. *59*, 671–679.

Corcoran, R.B., Dias-Santagata, D., Bergethon, K., et al. (2010). BRAF gene amplification can promote acquired resistance to MEK inhibitors in cancer cells harboring the BRAF V600E mutation. Sci. Signal. *3*, ra84.

Emery, C.M., Vijayendran, K.G., Zipser, M.C., et al. (2009). MEK1 mutations confer resistance to MEK and B-RAF inhibition. Proc. Natl Acad. Sci. USA *106*, 20411–20416.

Engelman, J.A., Chen, L., Tan, X., et al. (2008). Effective use of PI3K and MEK inhibitors to treat mutant Kras G12D and PIK3CA H1047R murine lung cancers. Nat. Med. *14*, 1351–1356.

Gopal, Y.N., Deng, W., Woodman, S.E., et al. (2010). Basal and treatment-induced activation of AKT mediates resistance to cell death by AZD6244 (ARRY-142886) in Braf-mutant human cutaneous melanoma cells. Cancer Res. *70*, 8736–8747.

Haura, E.B., Ricart, A.D., Larson, T.G., et al. (2010). A phase II study of PD-0325901, an oral MEK inhibitor, in previously treated patients with advanced non-small cell lung cancer. Clin. Cancer Res. *16*, 2450–2457.

Iadevaia, S., Lu, Y., Morales, F.C., et al. (2010). Identification of optimal drug combinations targeting cellular networks: integrating phospho-proteomics and computational network analysis. Cancer Res. *70*, 6704–6714.

Iverson, C., Larson, G., Lai, C., et al. (2009). RDEA119/BAY 869766: a potent, selective, allosteric inhibitor of MEK1/2 for the treatment of cancer. Cancer Res. *69*, 6839–6847.

Janne, P.A., Gray, N., and Settleman, J. (2009). Factors underlying sensitivity of cancers to small-molecule kinase inhibitors. Nat. Rev. Drug Discov. *8*, 709–723.

Kitano, H. (2007). A robustness-based approach to systems-oriented drug design. Nat. Rev. Drug Discov. *6*, 202–210.

Knight, Z.A., Lin, H., and Shokat, K.M. (2010). Targeting the cancer kinome through polypharmacology. Nat. Rev. Cancer *10*, 130–137.

Lehar, J., Krueger, A., Zimmermann, G., et al. (2008). High-order combination effects and biological robustness. Mol. Syst. Biol. *4*, 215.

Lemmon, M.A., and Schlessinger, J. (2010). Cell signaling by receptor tyrosine kinases. Cell *141*, 1117–1134.

LoRusso, P.M., Krishnamurthi, S.S., Rinehart, J.J., et al. (2010). Phase I pharmacokinetic and pharmacodynamic study of the oral MAPK/ERK kinase inhibitor PD-0325901 in patients with advanced cancers. Clin. Cancer Res. *16*, 1924–1937.

Mattoon, D.R., Lamothe, B., Lax, I., et al. (2004). The docking protein Gab1 is the primary mediator of EGF-stimulated activation of the PI-3K/Akt cell survival pathway. BMC Biol. *2*, 2–4.

Meads, M.B., Gatenby, R.A., and Dalton, W.S. (2009). Environment-mediated drug resistance: a major contributor to minimal residual disease. Nat. Rev. Cancer *9*, 665–674.

Mendoza, M.C., Er, E.E., and Blenis, J. (2011). The Ras-ERK and PI3K-mTOR pathways: cross-talk and compensation. Trends Biochem. Sci. *36*, 320–328.

Mirzoeva, O.K., Das, D., Heiser, L.M., et al. (2009). Basal subtype and MAPK/ERK kinase (MEK)-phosphoinositide 3-kinase feedback signaling determine susceptibility of breast cancer cells to MEK inhibition. Cancer Res. *69*, 565–572.

Montagut, C., Sharma, S.V., Shioda, T., et al. (2008). Elevated CRAF as a potential mechanism of acquired resistance to BRAF inhibition in melanoma. Cancer Res. *68*, 4853–4861.

Nazarian, R., Shi, H., Wang, Q., et al. (2010). Melanomas acquire resistance to B-RAF(V600E) inhibition by RTK or N-RAS upregulation. Nature *468*, 973–977.

Pacold, M.E., Suire, S., Perisic, O., et al. (2000). Crystal structure and functional analysis of Ras binding to its effector phosphoinositide 3-kinase gamma. Cell *103*, 931–943.

Papp, B., Notebaart, R.A., and Pal, C. (2011). Systems-biology approaches for predicting genomic evolution. Nat. Rev. Genet. *12*, 591–602.

Prahallad, A., Sun, C., Huang, S., et al. (2012). Unresponsiveness of colon cancer to BRAF(V600E) inhibition through feedback activation of EGFR. Nature *483*, 100–103.

Rinehart, J., Adjei, A.A., Lorusso, P.M., et al. (2004). Multicenter phase II study of the oral MEK inhibitor, CI-1040, in patients with advanced non-small-cell lung, breast, colon, and pancreatic cancer. J. Clin. Oncol. *22*, 4456–4462.

Rodriguez-Viciana, P., Warne, P.H., Dhand, R., et al. (1994). Phosphatidylinositol-3-OH kinase as a direct target of Ras. Nature *370*, 527–532.

Shin, S.Y., Yang, H.W., Kim, J.R., et al. (2011). A hidden incoherent switch regulates RCAN1 in the calcineurin-NFAT signaling network. J. Cell Sci. *124*, 82–90.

Solit, D.B., Garraway, L.A., Pratilas, C.A., et al. (2006). BRAF mutation predicts sensitivity to MEK inhibition. Nature *439*, 358–362.

Sordella, R., Bell, D.W., Haber, D.A., et al. (2004). Gefitinib-sensitizing EGFR mutations in lung cancer activate anti-apoptotic pathways. Science *305*, 1163–1167.

Suire, S., Hawkins, P., and Stephens, L. (2002). Activation of phosphoinositide 3-kinase gamma by Ras. Curr. Biol. *12*, 1068–1075.

Wagner, A. (2000). Robustness against mutations in genetic networks of yeast. Nat. Genet. *24*, 355–361.

Wee, S., Jagani, Z., Xiang, K.X., et al. (2009). PI3K pathway activation mediates resistance to MEK inhibitors in KRAS mutant cancers. Cancer Res. *69*, 4286–4293.

Wickenden, J.A., Jin, H., Johnson, M., et al. (2008). Colorectal cancer cells with the BRAF(V600E) mutation are addicted to the ERK1/2 pathway for growth factor-independent survival and repression of BIM. Oncogene *27*, 7150–7161.

Wildermuth, M.C. (2000). Metabolic control analysis: biological applications and insights. Genome Biol. *1*, REVIEWS1031.

Yeh, T.C., Marsh, V., Bernat, B.A., et al. (2007). Biological characterization of ARRY-142886 (AZD6244), a potent, highly selective mitogen-activated protein kinase kinase 1/2 inhibitor. Clin. Cancer Res. *13*, 1576–1583.